Planar GRIN Lenses for MEMS Energy Harvesters: A Macroscale Proof of Concept

Valentina Zega, Marco Antonacci, Attilio Frangi, Alberto Corigliano
Department of Civil and Environmental Engineering
Politecnico di Milano
Milano, Italy
valentina.zega@polimi.it, marco.antonacci@polimi.it.
attilio.frangi@polimi.it, alberto.corigliano@polimi.it

Emanuele Riva
Department of Mechanical Engineering
Politecnico di Milano
Milano, Italy
emanuele.riva@polimi.it

***Summary*—Phononic Crystal (PnC) Gradient Index (GRIN) lenses have been deeply studied in recent years for their promising applications in energy harvesting. Here, we propose the design and we show an experimental validation of a GRIN lens fully compatible with microfabrication processes that can be employed as Micro-Electro-Mechanical Systems (MEMS) energy harvester after proper miniaturization. Two refractive index gradient formation mechanisms are combined to boost the performances of the lens, thus achieving an amplification factor of 7.49x at the focal point that, to the Authors best knowledge, represents one of the best results available so far in the context of planar lenses. Numerical simulations and experimental tests performed on a macroscale prototype are in very good agreement.**

Keywords—GRIN lens; energy harvester; Phononic Crystals; wave focusing

I. Introduction

Acoustic Metamaterials (AM) and Phononic Crystals (PnC) are artificial materials properly designed to control and guide elastic/ acoustic waves in unprecedented ways. For this reason, acoustic metamaterials have been used and proposed for a large variety of applications of technological relevance, among which wave trappers [1], acoustic funnels [2], mirrors [3], vibration isolators [4], and lenses [5].

A relevant line of work employs PnCs for the functional design of elastic/acoustic lenses, which represents a promising solution for energy harvesting devices [6]. In other words, PnC lenses are able to focus (and thus amplify) input plane waves in the neighborhood of a point where, for example, the energy can be more efficiently collected through piezoelectric transducers.

More in detail, the design of high-performance PnC lenses is based on the PnC capability to tune the wave speeds over a desired frequency bandwidth, which is often accomplished through a variation of a geometrical or physical parameter along a relevant dimension.

Several examples of PnC GRIN lenses available in the literature [7]-[9] are obtained by modulating the refractive index through the local modification of the unit cell thickness [1], the inclusion diameter [10], the use of different materials [11], or through the modulation of the unit cell orientation [8]. This strategy is particularly effective for regions in the neighborhood of bandgap frequencies, i.e. frequency ranges where propagation of elastic/acoustic wavs is not permitted, where the dispersion diagram can take advantage of greater changes in response to the unit cell modulation.

In this work, we combine two different gradient refractive index formation mechanisms, i.e. modification of the unit cell hole dimension and orientation, to obtain a high-performance GRIN lens. Moreover, we chose a single-material and planar design, which is functional to a future implementation of the proposed lens as a MEMS energy harvester after proper miniaturization.

We achieve an amplification factor of 7.49x at the focal point which is, to the Authors best knowledge, one of the best results available so far for planar and single-phase GRIN lenses.

II. GRIN Lens Design

The GRIN lenses working principle is based on the well-known Snell's law, applied here to elasto-acoustic wave framework. To achieve the focusing effect, GRIN lenses are designed to provide a tailored refractive index profile along the vertical direction (y) which, in the case at hand, is a hyperbolic secant profile. The implementation of such a profile allows conveying waves in specific points distributed along the horizontal axis of symmetry of the structure, referred as focusing points in the following [12].

The equation describing the hyperbolic secant profile of the refractive index of a GRIN lens reads [13]:

$$n(y)=n_{max}\,\mathrm{sech}(\alpha y), \tag{1}$$

where n_{max} is the maximum refractive index that can be achieved through a specific design, y is the coordinate of the vertical axis and α is the gradient parameter that controls the position of the focusing point FP along the horizontal symmetry axis ($FP = \pi/2\alpha$) and the efficiency of the focusing effect. The refractive index $n(y)$ is finally computed as:

$$n(y) = \frac{v_{\Gamma M_{ref}}}{v_{\Gamma M_y}} \tag{2}$$

where $v_{\Gamma M_y}$ is the phase speed of a wave propagating within the PnC domain and along a given direction ΓM , i.e. the horizontal direction in physical space, calculated at the coordinate y of the GRIN lens. $v_{\Gamma M_{ref}}$ is the phase speed of the wave propagating

in the same direction in a homogeneous plate made of the same material.

A PnC is hereafter exploited to tune the waves phase speeds in the desired way and, hence, to obtain the desired hyperbolic secant profile of the refractive index.

Note that eq. (2) is valid only under the hypotheses of Snell's law, which are not always verified for PnCs being frequency dispersive and potentially anisotropic [11]. In our configuration we carefully designed the geometry to guarantee the validity of such hypotheses through the computation and verification of equi-frequency contours here not reported for the sake of brevity [10].

To that end, a hexagonal lattice with inner hole of characteristic dimension *a* is here chosen as geometry of the PnC GRIN lens (see Fig.1a). Thanks to its planar topology and single material constitution, the implementation represents a good candidate for applications in MEMS energy harvesters after proper miniaturization.

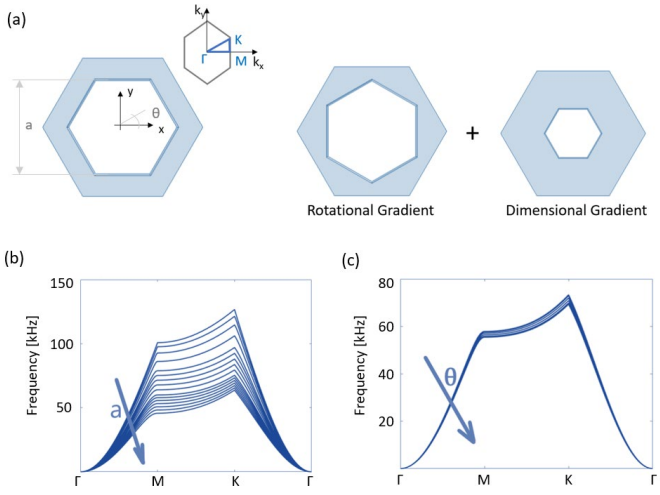

Fig.1 (a) Schematic view of the employed unit cell and the gradient index formation mechanisms. The Irreducible Brillouin Zone (IBZ) employed for the dispersion diagram computation is reported in the inset. Dispersion diagram computed for different (b) inner hole dimensions (a ∈ [0-7.75]mm with θ = 0°) and (c) orientations (θ ∈ [0 - 25]° with *a* = 7.75mm).

The hyperbolic secant refractive index profile needed to focus a propagating A_0 wave front is achieved through a two-step design procedure which is hereafter detailed. Firstly, the hole dimension is varied (Fig. 1a), thus mapping a refractive index that spans from n_{min} = 1 (relative to the continuous material) to $n=1.24$ (relative to the biggest hole feasible through the employed fabrication process, see Sec. III). Then, a rotational gradient (see Fig. 1a) is applied to the unit cells further widening the refractive index domain to n_{max}, thus improving the focusing capability of the lens.

Other relevant parameters include the size of the unit cell (1 cm) and the out-of-plane thickness of 4 mm. Iron is chosen as constitutive material thanks to its negligible damping and to the high resistance to thermal deformations induced by the fabrication process (see Section III). The corresponding material properties are E=210 GPa, ρ=7860 Kg/m^3 and ν=0.29.

The numerical dispersion analyses are carried out in COMSOL Multiphysics v. 5.6 for different holes dimensions and orientations. Bloch-Floquet boundary conditions are applied to the lateral surfaces of the unit cell to simulate infinite periodicity of the PnC, while stress-free boundary conditions are on the top and bottom surfaces to simulate the final plane geometry of the lens. By exploiting the hexagonal symmetry of the unit cell, the wave-vector is swept in the Irreducible Brillouin Zone (IBZ) reported in the top left corner of Fig. 1a. Flexural A_0 Lamb waves are isolated from the full dispersion diagram and reported in Fig. 1b-c for different dimensions and orientations of the unit cell inner hole, respectively.

Fixing a reference operating frequency, in this work equal to 30 kHz, from Fig. 1b we observe that by increasing the hole size *a*, the wavevector increases too. Hence, cells with bigger inclusions have a slower propagation speed. The same trend can be observed for the rotational gradient: rotating the inclusion from 0° to 25° reflects into a wave speed decrease. It is worth mentioning that the design frequency of 30 kHz is chosen here as an example, but different frequencies can be selected to fulfil specific applications.

According to eq. (2) and due to the dispersion diagrams shown in Fig. 1b-c, a refractive index spanning from 1 to 1.285 can be obtained through the combination of the hole dimensions and rotations variations in the ranges [0-7.75] mm and [0-25]°, respectively. Note that the maximum refractive index value is here limited by the fabrication process constraints (Section III), which requires a minimum distance between two neighbouring holes greater than 1 mm. A more accurate fabrication process, like MEMS micromachining, would enable to relax such constraints, thus improving the overall performances of the lens.

According to these findings, a PnC GRIN lens is designed as schematically reported in Fig.2. A close-up view of the patterned area is also reported to point-out the combination of the two refractive index gradient formation mechanisms exploited in this work. The focal point position is estimated equal to 21.28 cm from the left side of the lens. As a consequence, the lens footprint is chosen equal to 30 x 20 cm^2.

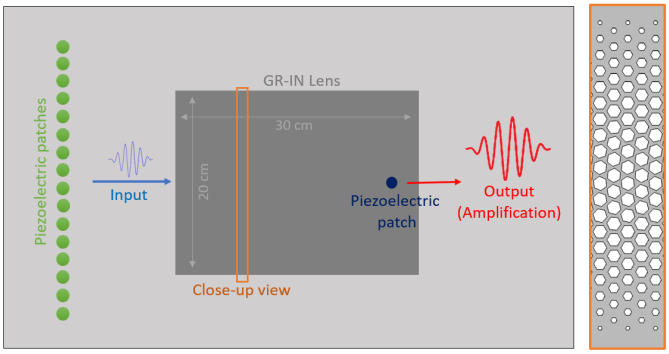

Fig.2 Schematic view of the GRIN lens designed, fabricated and tested in this work.

A set of piezoelectric patches is applied on the left side of the GRIN lens to generate an A_0 propagating wavefront (in the form of a plane wave), while an output piezoelectric patch is located at the focusing point to detect the amplified signal in view of energy harvesting applications. To guarantee the efficient generation of the input wavefront through the input

piezoelectric patches and to avoid undesired reflected waves, the lens is embedded in a wider domain as shown in Fig.2. Input piezoelectric patches are located 15 cm before the lens' left border to guarantee a proper generation of the wavefront. Each piezoelectric patch has a diameter of 15 mm, while the distance between patches is set equal to 17 mm.

To verify the focusing capability of the lens in a real case scenario, the dispersion and ray tracing analyses are replaced by transient simulations.

The multi-physics environment of COMSOL Multiphysics v. 5.6 is exploited to simulate the piezoelectric actuation and readout. A time step of $t = 8.883\ 10^{-7}$s is employed in compliance with the Courant, Friedrichs and Lewy (CFL) condition, while the spatial mesh dimension is chosen such as to correctly catch the smallest wavelength of the propagating waves ($\lambda = 3.47$ cm).

The input signal applied in series to the piezoelectric patches located on the left side of the lens consists of 6 cycle tone burst voltage signal of amplitude 50 V centred at 30 kHz which is the working frequency of the proposed PnC GRIN lens.

In Fig.3 numerical predictions of the normalized velocity field computed at $t = 2.38\ 10^{-4}$ s and at the time instant when focalization is expected ($t = 3.49\ 10^{-4}$ s) are reported. Normalized velocity is here obtained as the out-of-plane velocity of each point of the plate divided by the velocity computed in the homogeneous region on the left side of the lens at a time instant before the plane wave strikes the lens. From Fig. 3b it is clear that an amplification of 7.28 is expected at the focalization point, thus confirming the proposed design strategy.

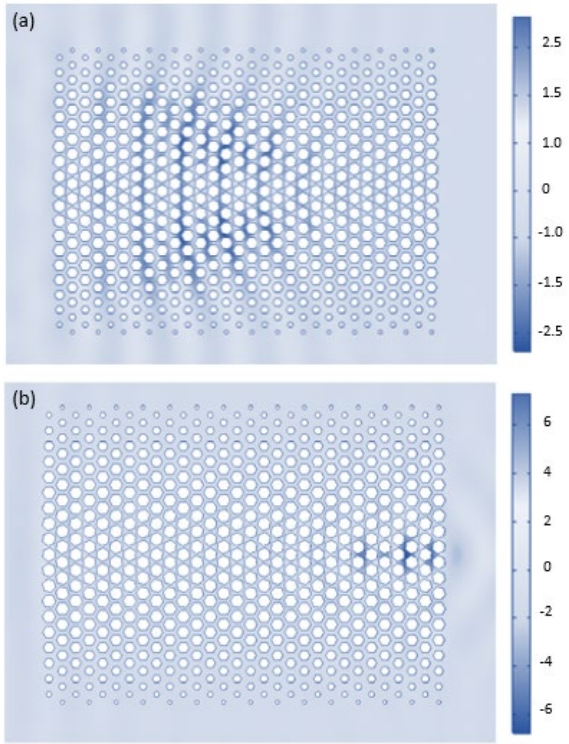

Fig.3 Numerical prediction of the normalized velocity field computed at the time instant (a) t= $2.38\ 10^{-4}$ s and (b) when focalization is experienced (t = $3.49\ 10^{-4}$ s).

III. Experimental Tests

Aware of the promising results obtained through analytical and numerical models, a macroscale prototype of the PnC GRIN lens is fabricated exploiting a laser cutting process on an iron plate of 4 mm thickness.

The prototype is suspended on an auxiliary frame to guarantee free-conditions at the boundaries, while piezoelectric patches are properly glued on the plate through a conductive glue to allow input generation and output readout. Fig.4 shows the experimental setup employed in the following. The same input used for numerical simulations is applied to all the piezoelectric patches located at the left side of the lens to guarantee the generation of a planar A_0 propagating wavefront. In particular, the burst signal is generated through a KEYSIGHT 33500B and amplified to 50V through a high-frequency amplifier.

During the experimental campaign, the lens was able to achieve an amplification factor of 7.49. The amplification factor is computed as the output signal measured by the piezoelectric patch glued on the focalization point whose position has been estimated through the time domain numerical analysis, divided by the input signal. In Fig.5 the amplification achieved at the focusing point by both numerical time domain analyses and experimental tests are reported. The agreement between experimental results and numerical predictions is satisfactory.

Note that the focusing point obtained in numerical predictions is located 1 cm apart from the analytical prediction. This is here considered an acceptable discrepancy, considering the simplifying hypotheses behind the analytical model and the dispersion analyses.

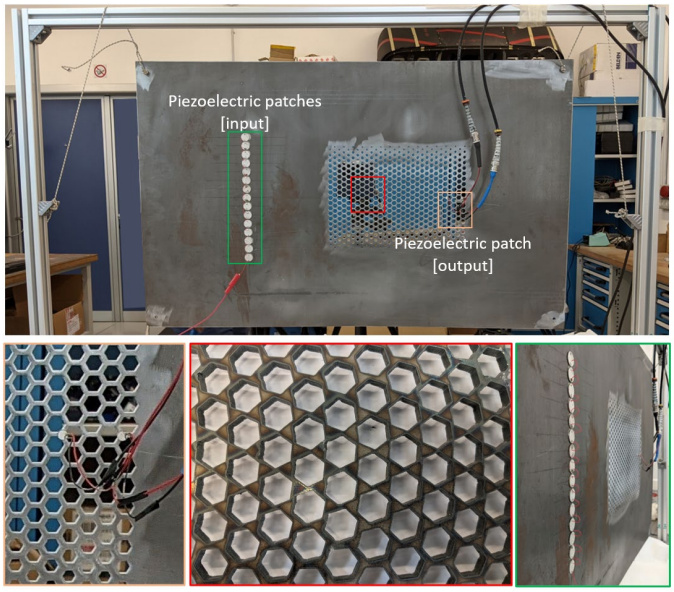

Fig.4 Experimental set-up employed for the measurements. Close-up view of the focusing area where the output piezoelectric patch is located, of the lens and of the input area with piezoelectric patches connected in series through wires.

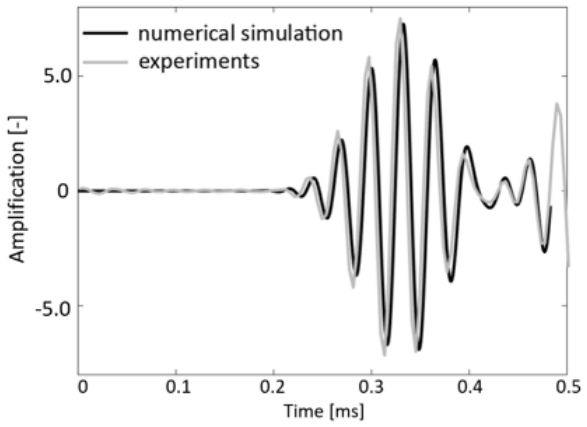

Fig.5 Voltage signal measured through the piezoelectric patch located at the focal point normalized with respect to the input voltage signal.

IV. CONCLUSIONS

In this work, a PnC GRIN lens is designed combining two refractive index gradient formation mechanisms: the variation of the inclusion dimensions and orientation.

Numerical analyses and experimental results performed on a macroscale prototype prove the design strategy and demonstrate an amplification factor of 7.49x at the focal point.

Thanks to the full compatibility of the proposed solution with standard micromachining processes, our work opens the path to a new class of MEMS energy harvesters based on PnC GRIN lenses.

Future work will be addressed to the miniaturization of these device concepts and to their fabrication and testing at the micro-scale.

ACKNOWLEDGMENTS

E.R. gratefully acknowledges the Italian Ministry of Education, University and Research for the support provided through the Project "Department of Excellence LIS4.0- Lightweight and Smart Structures for Industry 4.0."

REFERENCES

[1] Soo-Ho Jo et al. "A graded phononic crystal with decoupled double defects for broadband energy localization". In: International Journal of Mechanical Sciences 183 (2020), p. 105833. doi: 10.1016/j.ijmecsci.2020.105833.

[2] Matteo Carrara et al. "Metamaterial-inspired structures and concepts for elastoacoustic wave energy harvesting". In: Smart Materials and Structures 22.6 (2013), p. 065004. doi: 10.1088/0964-1726/22/6/065004.

[3] Matteo Carrara et al. "Dramatic enhancement of structure-borne wave energy harvesting using an elliptica acoustic mirror". In: Applied Physics Letters 100.20 (2012), p. 204105. doi: 10.1063/1.4719098.

[4] Luca D'Alessandro, Edoardo Belloni, Raffaele Ardito, Francesco Braghin, Alberto Corigliano "Mechanical low-frequency filter via modes separation in 3D periodic structures" Appl. Phys. Lett. 111 (2017), p. 231902. doi: 10.1063/1.4995554.

[5] Tol Serife, Fahrettin Levent Degertekin, and Alper Erturk. "Phononic crystal Luneburg lens for omnidirectional elastic wave focusing and energy harvesting". In: Applied Physics Letters 111.1 (2017), p. 013503. doi: 10.1063/1.4991684.

[6] Jacopo Iannacci. "Microsystem based Energy Harvesting (EH-MEMS): Powering pervasivity of the Internet of Things (IoT): A review with focus on mechanical vibrations". In: Journal of King Saud University -Science 31.1 (2019), pp. 66_74. doi: 10.1016/j.jksus.2017.05.019.

[7] Yabin Jin et al. "Simultaneous control of the S0 and A0 Lamb modes by graded phononic crystal plates" In: Journal of Applied Physics 117.24 (2015), p. 244904. doi: 10.1063/1.4923040.

[8] Yuping Tian et al. "Phononic crystal lens with an asymmetric scatterer". In: Journal of Physics D: Applied Physics 52.2 (2018), p. 025102. doi: 10.1088/1361-6463/aae679.

[9] Yabin Jin, Bahram Djafari-Rouhani, and Daniel Torrent. "Gradient index phononic crystals and metamaterials". In: Nanophotonics 8.5 (2019), pp. 685_701. doi: 10.1515/nanoph-2018-0227.

[10] Tol Serife, Fahrettin Levent Degertekin, and Alper Erturk. "Gradient-index phononic crystal lens-based enhancement of elastic wave energy harvesting". In: Applied Physics Letters 109.6 (2016), p. 063902. doi: 10.1063/1.4960792.

[11] Sz-Chin Steven Lin et al. "Gradient-index phononic crystals". In: Physical Review B 79.9 (2009), p. 094302. doi: 10.1103/PhysRevB.79.094302.

[12] Ahmad Zareei et al. "Continuous profile flexural GRIN lens: Focusing and harvesting flexural waves". In: Applied Physics Letters 112.2 (2018), p. 023901. doi: 10.1063/1.5008576.

[13] Alfonso Climente, Daniel Torrent, and Jose Sanchez-Dehesa. "Sound focusing by gradient index sonic lenses". In: Applied Physics Letters 97.10 (2010), p. 104103. doi: 10.1063/1.3488349.